Journal of The
Electrochemical Society

Monolayer Honeycomb Borophene: A Promising Anode Material with a Record Capacity for Lithium-Ion and Sodium-Ion Batteries

To cite this article: Jingzhen Li *et al* 2020 *J. Electrochem. Soc.* **167** 090527

Journal of The Electrochemical Society, 2020 **167** 090527

Monolayer Honeycomb Borophene: A Promising Anode Material with a Record Capacity for Lithium-Ion and Sodium-Ion Batteries

Jingzhen Li,[1,2] Georgios A. Tritsaris,[2] Xiuying Zhang,[1] Bowen Shi,[1] Chen Yang,[1,3] Shiqi Liu,[1] Jie Yang,[1] Linqiang Xu,[1] Jinbo Yang,[1,4,5] Feng Pan,[6,*] Efthimios Kaxiras,[2,7,z] and Jing Lu[1,4,5,z]

[1]*State Key Laboratory for Mesoscopic Physics and Department of Physics, Peking University, Beijing 100871, People's Republic of China*
[2]*John A. Paulson School of Engineering and Applied Sciences, Harvard University, Cambridge, Massachusetts 02138, United States of America*
[3]*Academy for Advanced Interdisciplinary Studies, Peking University, Beijing 100871, People's Republic of China*
[4]*Collaborative Innovation Center of Quantum Matter, Beijing 100871, People's Republic of China*
[5]*Key Laboratory for the Physics and Chemistry of Nanodevices, Department of Electronics, Peking University, Beijing 100871, People's Republic of China*
[6]*School of Advanced Materials, Peking University, Shenzhen Graduate School, Shenzhen 518055, People's Republic of China*
[7]*Department of Physics, Harvard University, Cambridge, Massachusetts 02138, United States of America*

Two-dimensional (2D) materials are a promising candidate for the anode material of lithium-ion battery (LIB) and sodium-ion battery (NIB) for their unique physical and chemical properties. Recently, a honeycomb borophene (*h*-borophene) has been fabricated by molecular beam epitaxy (MBE) growth in ultra high vacuum. Here, we adopt the first-principles density functional theory calculations to study the performance of monolayer (ML) *h*-borophene as an anode material for the LIB and NIB. The binding energies of the ML *h*-borophene-Li/Na systems are all negative, indicating a steady adsorption process. The diffusion barriers of the Li and Na ions in *h*-borophene are 0.53 and 0.17 eV, respectively, and the anode overall open-circuit voltages for the LIB and NIB are 0.747 and 0.355 V, respectively. The maximum theoretical storage capacity of *h*-borophene is 1860 mAh·g^{-1} for NIB and up to 5268 mAh·g^{-1} for LIB. The latter is more than 14 times higher than that of commercially used graphite (372 mAh·g^{-1}) and is also the highest theoretical capacity among all the 2D materials for the LIB discovered to date. Our study suggests that *h*-borophene is a promising anode material for high capacity LIBs and NIBs.
 [DOI: 10.1149/1945-7111/ab8a9b]

Manuscript submitted January 12, 2020; revised manuscript received April 1, 2020. Published April 27, 2020. *This paper is part of the JES Focus Issue on Battery Safety, Reliability and Mitigation.*

Supplementary material for this article is available online

With the increasing demand of the performance for environmentally friendly electric vehicles and improving requirements of the stability for the portable electric device, the rechargeable batteries with high capacity, superior energy density, high power density, and long cycle life are in urgent demand.[1] Lithium-ion battery (LIB) is one of the most widely used rechargeable batteries because of its lightweight, small size and good safety.[2–4] Due to the limitation of the reserves of lithium (Li) element on Earth, the abundant reserves of sodium (Na) element also stimulate the research interests of low-cost sodium-ion battery (NIB) of the scientists.[5–7] To further satisfy the rapid development of the energy storage market demands, we make an effort to seek the LIBs and NIBs with better performance. Generally, one of the most efficient ways to improve the performance of the LIBs and NIBs is to find new anode materials to take the place of the commercial graphite anode with a relatively low theoretical specific capacity of 372 mAh·g^{-1}.[4,8,9]

2D materials are regarded as promising candidates of anode materials of the LIB and NIB due to several advantages:[10–12] (i) a small volume expansion related to their thin atomic thickness resulting in a good cyclability, (ii) a low diffusion barrier associated with a few dangling bonds at the surface leading to a high charge-discharge rate, (iii) a low absolute value of binding energy pertaining to surface weak interaction causing a proper open-circuit voltage of the anode, (iv) a high surface-to-mass ratio leading to abundant adsorption sites corresponding to a high capacity. Many first-principles calculations study the properties of 2D materials as anode materials of the LIB or NIB,[13–34] and these 2D materials all present higher specific capacities and lower diffusion barriers than conventional graphite, such as graphene and graphdiyne.[4,8,9,13,14,17] Experimentally, the capacities of graphdiyne-based LIB, graphene hybrid-based LIB and SnS/graphene-based NIB are found to be 901, 784 and 940 mAh·g^{-1}, respectively,[35–37] and these experimental results generally coincide well with previous theoretical findings.[13,14,17]

Borophene, a new type of III group 2D materials, has been theoretically predicted with 16 different types by the structural searching method,[38] and it has been shown to exist on the Ag (111), Au (111) and Cu (111) surfaces by using first-principles calculations.[39,40] The 2D monolayer (ML) borophene with 2-*Pmm* symmetry on the Ag (111) substrate has been successfully synthesized in 2015 for the first time.[41] Independently, Feng et al. also used molecular beam epitaxy (MBE) to grow another two boron sheets (named as β_{12} and χ_3) on the Ag (111) surface.[42] By employing MBE growth, Li et al. successfully fabricated an attractive 2D ML honeycomb borophene (*h*-borophene) by choosing an Al (111) surface as the substrate in 2018.[43] Very recently, Wu et al. reported the production of large-area borophene up to 100 μm^2 on the Cu (111) surface.[44] Subsequently, Kiraly et al. synthesized the sixth kind of borophene growing on the Au (111) surface.[45] The above six kinds of borophenes are metallic. Due to their good electric conductivity, lightweight and inheritance excellent property from 2D materials, borophene is naturally considered as a suitable alternative electrode material of the energy storage device, especially in the LIB or NIB. A series of density functional theory (DFT) results of borophene adsorption and diffusion properties are calculated and show that borophene is a suitable anode material of the LIB/NIB.[46–51] The few-layer borophene-based capacity device exhibits impressive electrochemical performance with a wide

*Electrochemical Society Member.
[z]E-mail: kaxiras@physics.harvard.edu; jinglu@pku.edu.cn

potential window of up to 3.0 V, excellent energy density as high as 46.1 Wh kg^{-1} at a power density of 478.5 W kg^{-1} and excellent cycling stability with 88.7% retention of the initial specific capacitance after 6000 cycles, indicating good performance of borophene energy storage device.[52] However, the adsorption ability of the Li and Na ions on *h*-borophene has not been investigated. Among all the existing borophene, *h*-borophene with non-buckled structure has the least molar mass per unit cell and the highest density of hexagonal hole offering more adsorption sites, suggestive of a higher capacity than any other phases of borophene. Hence, it is very important to understand the Li and Na ions adsorption and diffusion properties of *h*-borophene as an anode material.

In this article, we study the adsorption and diffusion processes of the Li and Na ions on the surface of ML *h*-borophene through the first-principles DFT calculations and obtain three important parameters (the diffusion barrier height, the average OCV and the maximum theoretical storage capacity) to evaluate the performance of the LIB and NIB. We find that the Li and Na atoms prefer to stay in the hollow site (H site) on ML *h*-borophene. The maximum theoretical storage capacity for the ML *h*-borophene based LIB is 5268 mAh·g^{-1}, which is more than 14 times larger than that of the commercially used graphite-based LIB (372 mAh·g^{-1}).[4,53] The theoretical specific capacity of the ML *h*-borophene based NIB (1860 mAh·g^{-1}) is 53 times as high as that of graphite-based NIB (35 mAh·g^{-1}).[54] The estimated average OCVs of the ML *h*-borophene based LIB and NIB are 0.747 and 0.355 V, respectively. At the end of the discussion part, we compare the theoretical performance parameters of ML *h*-borophene as an anode material for the LIB/NIB with those of other ML 2D materials.[15–34]

Computational Methods

All Calculations were carried out using DFT in connection with the exchange correlation energy described by the generalized gradient approximation (GGA)[55–57] in the scheme proposed by Perdew–Burke–Ernzerhof (PBE)[58] as implemented in the Vienna ab initio simulation package (VASP).[59–61] The periodic boundary conditions are applied in three directions (x, y and z directions),[62] and a vacuum space of at least 20 Å in the *z* direction is used to simulate ML *h*-borophene to avoid image-image interactions. The projector-augmented wave (PAW) method with a cutoff energy of 400 eV is employed in our study.[63] Van der Waals interaction is taken into account using the semi-empirical dispersion correction of DFT-D3 approach.[64] The Methfessel–Paxton smearing with order $N = 1$ method was employed for ions relaxation of Li/Na atom-ML h-borophene system with a recommendation width of 0.2 eV. For this step, a *k*-mesh density of 0.02 $Å^{-1}$ under the Monkhorst-Pack method is sampled in the Brillouin zone with convergence threshold 10^{-5} eV for energy and 0.01 eV $Å^{-1}$ for force.[65] The tetrahedron smearing method with a width of 0.01 eV was employed for a single point calculation to obtain the PDOS and very accurate total energy values. The climbing image nudged elastic band (CI-NEB) method implemented in VASP transition state tools is used to determine the metal cationic minimum energy diffusion pathways and the corresponding energy barriers.[66] In this step, the algorithm to relax the ions into their energy minimization transition state is required in agreement with the previous calculation of initial and final state. We adopt completely same *k*-mesh density and convergence accuracy as ion relaxation both in the single point calculations and transition state calculations. The first-principles molecular dynamics (FPMD) simulations are performed using Nosé-Hoover thermostat employed in the canonical-ensemble at the finite temperatures with a time step of 1 fs and a $3 \times 3 \times 1$ *k*-point meshes.[67,68]

Results and Discussion

Crystal structures and adsorption ability of an isolated Li/Na atom on ML h-borophene.—The pristine lattice parameter of ML *h*-borophene is a = 3.0 Å with two borium (B) atom sites (as shown in Fig. 1a), which is in good agreement with the previous experimental report.[43] Before we studied the adsorption ability of the Li/Na atom adsorbed system, the stability of the isolated ML *h*-borophene should be confirmed first. We evaluate the stability of ML *h*-borophene by calculating the average formation energy (E_{form}) defined as $E_{form} = E_B - E_{tot}$, where E_B is the energy of an isolated B atom, and E_{tot} is the total energy per atom of ML borophene. The average formation energy of ML *h*-borophene is the lowest one (5.29 eV $atom^{-1}$) among all the studied ML borophenes including ML 2-*Pmm* (6.11 eV $atom^{-1}$), β_{12} (6.15 eV $atom^{-1}$), X_3 (6.16 eV $atom^{-1}$) and β_{1S} (6.08 eV $atom^{-1}$) borophene, but the positive average formation energy value of ML *h*-borophene still shows a certain degree of stability. The structural parameters and the average formation energy are listed in Table SI (available online at stacks.iop.org/JES/167/090527/mmedia) of supplementary materials. To further demonstrate the stability of the isolated ML *h*-borophene, we perform the FPMD simulation of ML *h*-borophene, and the isolated ML *h*-borophene is with small deformation at 500 K for 5 ps (as shown in Fig. 6a). The structural snapshot reveals that the isolated ML *h*-borophene has a good thermodynamic stability.

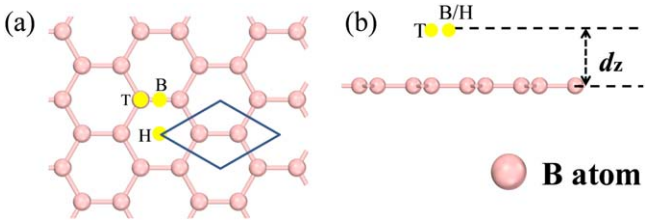

Figure 1 (a) Side and (b) top view of the freestanding ML *h*-borophene. The yellow dots indicate three high symmetry adsorption sites (B, T, H sites). The rhombus indicates the outline of the pristine unit cell of ML *h*-borophene. d_z is the distance between the adsorption atom to the ML *h*-borophene surface.

Then it is important to know exactly the favorable adsorption sites to evaluate the adsorption ability of an isolated Li/Na atom on the ML *h*-borophene surface. We use a 2×2 ML *h*-borophene supercell with one Li/Na atom located on to investigate the adsorption properties, and such a supercell is large enough to avoid the interaction between the Li/Na atoms in the adjacent periodic structure. Three types of high symmetry adsorption sites are considered (as shown in Fig. 1a): the hollow site above the center of the hexagon (H site), the bridge site on the bond of B-B (B site) and the atom point site on the top of a B atom (T site). After geometric optimization, all the studied Li/Na atoms remain in their initial place except for the Li at an initial bridge site. The adsorbed Li at the bridge site would automatically shift to the hollow site. The total energy of a Li/Na atom adsorbed on the H site of 2×2 ML *h*-borophene is the lowest one among that of a Li/Na atom adsorbed on the H, B and T sites, and the exact total energy of each corresponding structure is summarized in Table I.

To evaluate the adsorption ability of the Li and Na atoms on ML *h*-borophene, the binding energy (E_b) can be defined as

$$E_b = (E_{MnB8} - E_{B8} - nE_M)/n \quad [1]$$

where E_{MxB8}, E_{B8} and E_M are the total energy of the 2×2 ML *h*-borophene adsorbed by the metal atoms, pristine 2×2 ML *h*-borophene and per metal atom (M = Li or Na) in bulk of metal, respectively, and *n* is the number of metal atoms adsorbed on 2×2 ML *h*-borophene. According to Eq. 1, the lower binding energy of the Li/Na atom adsorbed on ML *h*-borophene is, the more favorable exothermic and spontaneous reaction between the Li/Na atom and ML *h*-borophene is. E_b's of the Li and Na ions adsorbed on the H site are −1.06 and −0.68 eV $atom^{-1}$, respectively. Those on the T site are −0.50 and −0.48 eV $atom^{-1}$, respectively. E_b of the Na ion adsorbed on the B site is −0.50 eV $atom^{-1}$. The values of E_b of different adsorption sites are collected in Table I. The absolute values of E_b on the H site are all larger than those of the B and T sites, indicating both the Li and Na ions preferring to stay on the H

Table I. Summary of the adsorption ability of an isolated Li/Na atom on ML *h*-borophene. d_a is the minimum Li/Na-B atom-to-atom distance projected in the z direction. E_t is the total energy of the ML *h*-borophene-Li/Na adsorption system. E_b is the average energy (per Li/Na atom) required to remove the Li/Na atoms from ML *h*-borophene. Charge transfer is the number of electrons losing from the Li/Na atom to ML *h*-borophene.

	Li atom			Na atom		
Adsorption site	Hollow	Bridge	Top	Hollow	Bridge	Top
Adsorpting distance d_a (Å)	1.41	—	2.11	1.99	2.30	2.41
Total energy E_t (eV)	−46.89	—	−46.33	−45.90	−45.72	−45.70
Binding energy E_b (eV atom^{-1})	−1.06	—	−0.50	−0.68	−0.50	−0.48
Charge transfer (e^-)	0.84	—	0.88	0.76	0.79	0.79

site. Thus, the following studies concentrate on the H site configurations. The distances from the Li/Na atoms at the H site to the ML *h*-borophene layer (d_Z) (Fig. 1b) are 1.41 (Li) and 1.99 (Na) Å. The Na atom has the larger distance to the surface of ML *h*-borophene and also the smaller binding energy with ML *h*-borophene. The absolute values of the E_b for Li (−1.10 eV atom^{-1}) and Na (−0.46 eV atom^{-1}) atom adsorbed on graphene are comparable to those on ML *h*-borophene,[69] indicating the stability of the Li/Na atoms-ML *h*-borophene systems. The binding energy is not corrected with zero-point energy and entropy contributions. Such kind of corrections could change the relative stability of the configurations with close total energy, but we do not expect the relative energy relation between the H and T (B) sites will be affected because of the large energy difference between the H and T (B) sites.

Diffusion of Li and Na ions on the ML h-borophene surface.— One of the most important parameters to evaluate the performance of the LIB/NIB is the charge-discharge rate, namely the Li/Na ions mobility on the host material. The high charge-discharge rate reflects a good rate capability of the LIB/NIB. Usually, we obtain the charge-discharge rate by estimating the molecular diffusion constant (D) of the metal ions. D is temperature-dependent and positively related to the ion mobility μ. As described by the Arrhenius equation,[18,27,70]

$$\mu \propto D = d^2 \cdot \upsilon \cdot \exp\left(\frac{-E_a}{k_B T}\right) \quad [2]$$

where d, υ, E_a and k_B are the diffusion distance of the Li/Na ion, the frequency of the hoping process, the diffusion barrier height (the activation energy) and Boltzmann's constant, respectively, and T is the environmental temperature. A high charge-discharge rate is related to a large ion mobility, corresponding to a low diffusion barrier height. To study the diffusion barrier of the Li/Na ion on ML *h*-borophene, we examine the optimal diffusion path along the zigzag and armchair directions of ML *h*-borophene.

The expecting pathways along both the zigzag (H → B → H) (as shown in Fig. 2a) and the armchair directions (H → T → B → T → H) (as shown in Fig. 2b) between two nearest neighboring H sites (the most favorite binding sites) are explored by considering the high structural symmetry of ML *h*-borophene. The diffusion energy profiles along the zigzag and armchair directions are illustrated in Figs. 2c and 2d, respectively. The diffusion barrier height along the zigzag direction is 0.53 and 0.17 eV for the Li and Na ions, respectively, and the corresponding pathway lengths are both about 3.69 Å (Fig. 2c). Along the zigzag direction, the B site is the maximum state as shown in the energy profile (Fig. 2c) and is energetically higher than the H site by about 0.53 and 0.17 eV for the Li and Na ions, respectively. The diffusion barrier height along the armchair direction is 0.54 and 0.19 eV for the Li and Na ions, respectively, and the corresponding pathway lengths are both about 5.90 Å (Fig. 2d). Along the armchair direction, the B site is the intermediate state as shown in the energy profile and is also energetically higher than the H site by about 0.53 and 0.17 eV for the Li and Na ions, respectively. The T site is the transition state, as shown in the energy profile and is energetically higher than the H site by about 0.54 and 0.19 eV for Li and Na ions, respectively. Although the diffusion barrier height of the Li/Na ion is not very apparent dependent on the diffusion path, the corresponding diffusion pathway length of the Li/Na ion along the zigzag is shorter than that along the armchair direction. Besides, the density of the diffusion barrier (determined by ratio of the number of the diffusion barrier height with a height of over 0.5 (for Li)/0.15(for Na) eV to the corresponding pathway length) along the zigzag direction is also less than that along the armchair direction. Obviously, the Li and Na ions prefer to migrate along the zigzag direction than the armchair direction on ML *h*-borophene because of the lower diffusion barrier height, the shorter pathway length and the lower density of the high diffusion barrier.

The Li ion has a higher diffusion barrier height than that of the Na ion and thus migrates harder on the ML *h*-borophene surface. But the diffusion barrier height of the Li ion on ML *h*-borophene (0.53 eV) is still smaller than those on ML β_{12} (0.66 eV) and χ_3 (0.60 eV) borophene[46] and comparable to some well-known anode materials including TiO_2-based polymorphs (∼0.5 eV)[71] and silicon (0.57 eV).[72] The diffusion barrier of the Na ion on ML *h*-borophene with a height of 0.17 eV is smaller than those on many other 2D materials, such as ML MoS_2 (0.68 eV),[25] MoN_2 (0.56 eV),[31] χ_3 borophene (0.34 eV),[46] β_{12} borophene (0.33 eV),[46] NiC_3 (0.23 eV)[22] and TiC_3 (0.18 eV),[73] suggesting a high charge-discharge rate of the ML *h*-borophene based NIB. We can conclude that the diffusion barrier height of the Na ion is 0.36 eV lower than that of the Li ion, and both the Li and Na ions on ML *h*-borophene have high ion mobilities and good rate capabilities of the LIB and NIB because of the relatively low diffusion barriers. Based on the discussion above, we make an effort to obtain the diffusion constant of the Li/Na ion on ML *h*-borophene by using Eq. 2. Here, we use the diffusion distance along the zigzag direction with the value of 3.69 Å as d, and the hoping frequency υ is taken from a typical value of 10^{13} s^{-1}. At the 300 K, the diffusion constant D values of the Li and Na ions on ML *h*-borophene are 1.72×10^{-11} and 1.90×10^{-5} cm^2 s^{-1}, respectively. The diffusion constant of the Li ion on ML *h*-borophene is one order of magnitude larger than that of c-Si (3.60×10^{-12} cm^2 s^{-1}).[74]

Li/Na storage capacities of ML* h-*borophene and average open-circuit voltages.— The maximum theoretical storage capacity is a highly important indicator to evaluate the performance of the LIB/NIB. To estimate the maximum capacity as reasonable as we can, the anode material should satisfy several requirements: i) It should adsorb the Li/Na ions as much as possible until its highest concentration; ii) Before reaching the maximum concentration of the Li/Na ions, the binding energy (calculated by the Eq. 1) of each concentration is negative; iii) The structure of the anode materials do not have irreversible deformation; iv) There is no Li/Na ion pushed out of the anode material surface.[15,50] Here, we employ the 2 × 2 supercells of ML *h*-borophene with an increasing Li/Na ion on both sides of the host material. We only increase one metal atom each

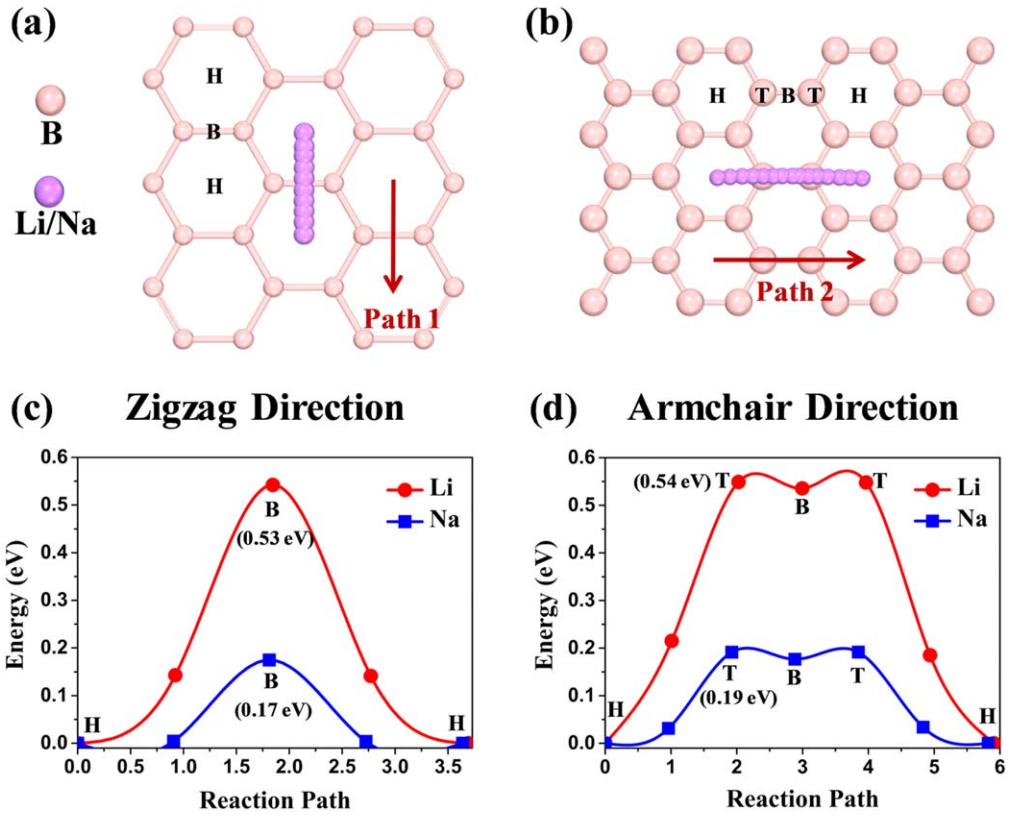

Figure 2. Li/Na-ion diffusion pathways along the zigzag (a) and armchair (b) direction. Diffusion energy barrier profile of Li and Na-ions on the surface of 2 × 2 ML *h*-borophene along the zigzag (c) and armchair (d) direction pathways.

time to obtain the next step concentration to obtain the sensitive average adsorption energy during the whole processing with the concentration smaller than 1. The charge/discharge processing can be described by the following half-cell reaction:

$$B_8 + nM^+ + ne^- \leftrightarrow M_nB_8 \quad [3]$$

Where M = (Li, Na), and n is the number of adsorbed metal ions. The average adsorption energy of each concentration can be described by Eq. 1. A negative value of the average adsorption energy indicates that the Li/Na ions in the LIBs/NIBs prefer to get adsorbed on the *h*-borophene surface, whereas a positive value of the adsorption energy means that the Li/Na ions are hard to get adsorbed on the *h*-borophene surface during the charging process.

To obtain the maximum adsorption concentration of the Li/Na ions adsorbed on the 2 × 2 ML *h*-borophene surface, we gradually increase the number of the Li/Na ions on the *h*-borophene surface. The concentration of the Li/Na ions adsorbed on the *h*-borophene surface is represented by the Li_xB/Na_xB. The x values of the Li_xB are 0.125, 0.25, 0.375, 0.5, 0.625, 0.75, 0.875, 1.000, 1.250, 1.750, 2.000 and 2.125 corresponding to the Li_1B_8, Li_2B_8, Li_3B_8, Li_4B_8, Li_5B_8, Li_6B_8, Li_7B_8, Li_8B_8, $Li_{10}B_8$, $Li_{14}B_8$, $Li_{16}B_8$ and $Li_{17}B_8$, respectively. According to the previous calculation of the most stable adsorption site of the Li/Na ions on the ML *h*-borophene surface, we only consider the Li/Na ions adsorbed on the H sites of both sides of the 2 × 2 ML *h*-borophene surface. After the H sites fully adsorbed, we put the Li ions on the T sites to continually increasing the concentration x from 1 to 2.125. Firstly, we calculate the different adsorption structures of the Li ions with the same concentration x and get the structure with the lowest total energy among all configurations at this concentration. Secondly, we calculate the binding energy of the lowest total energy configuration to check the stability of the systems after adsorbed the metal atoms

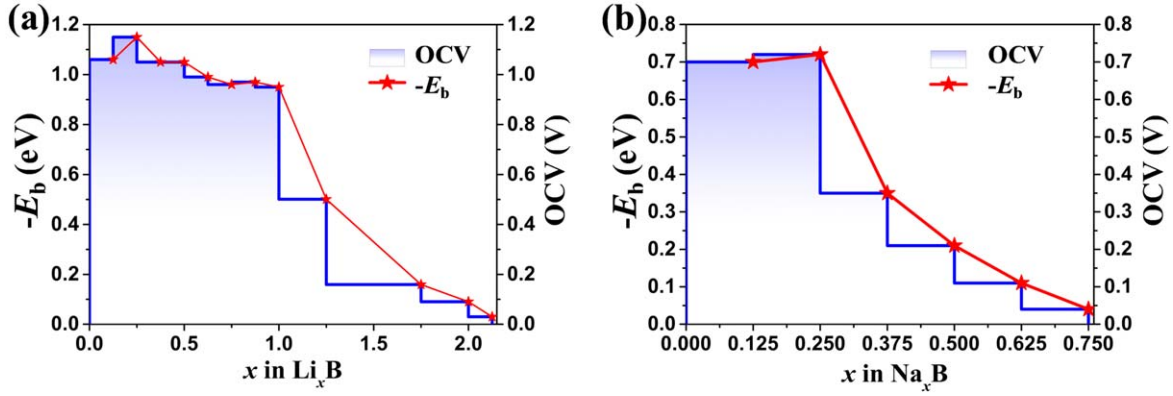

Figure 3. Negative binding energies ($-E_b$) (marked in red) and open-circuit voltage (OCV) profiles (marked in blue) as the function of (a) Li concentration x in Li_xB and (b) Na concentration x in Na_xB.

using Eq. 1. After the top two steps, we found that with the concentration x of the Li ions increasing from 0.125 to 2.125, the binding energy E_b (as shown in Fig. 3a) increases from −1.07 to −0.03 eV atom^{-1}, indicating the instability of the high concentration system. The most stable configurations of the adsorbed Li ions on the 2 × 2 ML *h*-borophene surface at the concentrations from 0.125 to 1 and 1.25 to 2.125 are listed in Figs. 4a–4h and 5a–5d, respectively, and no obvious deformation happens to ML *h*-borophene in these Li ion adsorption systems. Combining the binding energy E_b and the degree of deformation of ML *h*-borophene, we can conclude that the maximum concentration (x_{max}) of the lithiation process is at the value of 2.125.

Due to the structure of the $Li_{2.125}B$ owning a strategic concentration in our cases, it is necessary to give some detailed description of its structure. Figure 5d is the structure of the concentration of the $Li_{2.125}B$. We adopt the 2 × 2 ML *h*-borophene supercells, and the system actually contains eight B atoms and 17 li atoms. The initial structure of the $Li_{2.125}B$ has nine Li atoms above the ML *h*-borophene layer and eight Li atoms below the ML *h*-borophene layer, so the chemical environment on two sides of ML *h*-borophene is not the same. The different chemical environment of both sides of ML *h*-borophene results in the different adsorption behaviors of the Li ions. The distance between the lowest Li ion of the second Li layer and the first Li layer is 1.87 Å, and this distance can be regarded as the minimum distance between the two Li layers. However, the distance between the squeezed out Li ion and the second Li layer is 1.64 Å, and it is smaller than the minimum distance of two Li layers (1.87 Å). Therefore, the uppermost Li ion belongs to the second Li layer after carefully check its interlayer distance.

For the NIB, the x values of the Na_1B_8, Na_2B_8, Na_3B_8, Na_4B_8, Na_5B_8 and Na_6B_8 are 0.125, 0.250, 0.375, 0.500, 0.625 and 0.750, respectively. The matching binding energy E_b is shown in Fig. 3b, and the Na_7B_8 with a positive E_b determines that the maximum concentration (x_{max}) of the Na ion adsorbed on the 2 × 2 ML h-borophene surface is at the value of 0.750. The most stable configurations of the $Na_{0.125}B$, $Na_{0.25}B$, $Na_{0.375}B$, $Na_{0.5}B$, $Na_{0.625}B$ and $Na_{0.75}B$ are shown in Figs. S1a–S1f. From the optimized structure illustrated by Figs. 4–5 and S1a–S1f, ML *h*-borophene does not suffer from an apparent structural change, indicating a good rechargeable recycle property of the LIB/NIB.

As we mentioned before, the maximum theoretical storage capacity (C) is an important parameter to evaluate the performance of the LIB/NIB and is highly focused on its improvement. It depends on the concentration (x) of the Li/Na ions adsorbed on the 2 × 2 *h*-borophene surface and can be calculated by:

$$C = x_{max} F / M_B \quad [4]$$

Where x_{max} is the maximum concentration of M_xB (M = Li or Na), and F is the Faraday constant with a value of 26801.48 mAh mol^{-1}, and M_B is the Molar Mass of one B atom (10.811 g mol^{-1}). Generally speaking, F and M_B could be regarded as constant in a certain system, and thus the maximum theoretical storage capacity C is totally determined by the maximum concentration. The binding energy will be weaker with the increasing of the Li/Na ion concentration. The judgment of the maximum concentration is that the binding energy of the system is near zero. The higher the concentration of Li/Na ions is, the higher the capacity will be. In our studied systems, the calculated maximum theoretical storage capacity C is extremely high with a value of 5268 mAh·g^{-1} for the LIB and 1860 mAh·g^{-1} for the NIB. It is noteworthy that the maximum theoretical storage capacity C of the LIB for ML *h*-borophene as an electrode is the highest capacity among all reported 2D materials, and the comparison with other 2D anode materials will be discussed at the end of this part. We also defined the volumetric capacity C_v

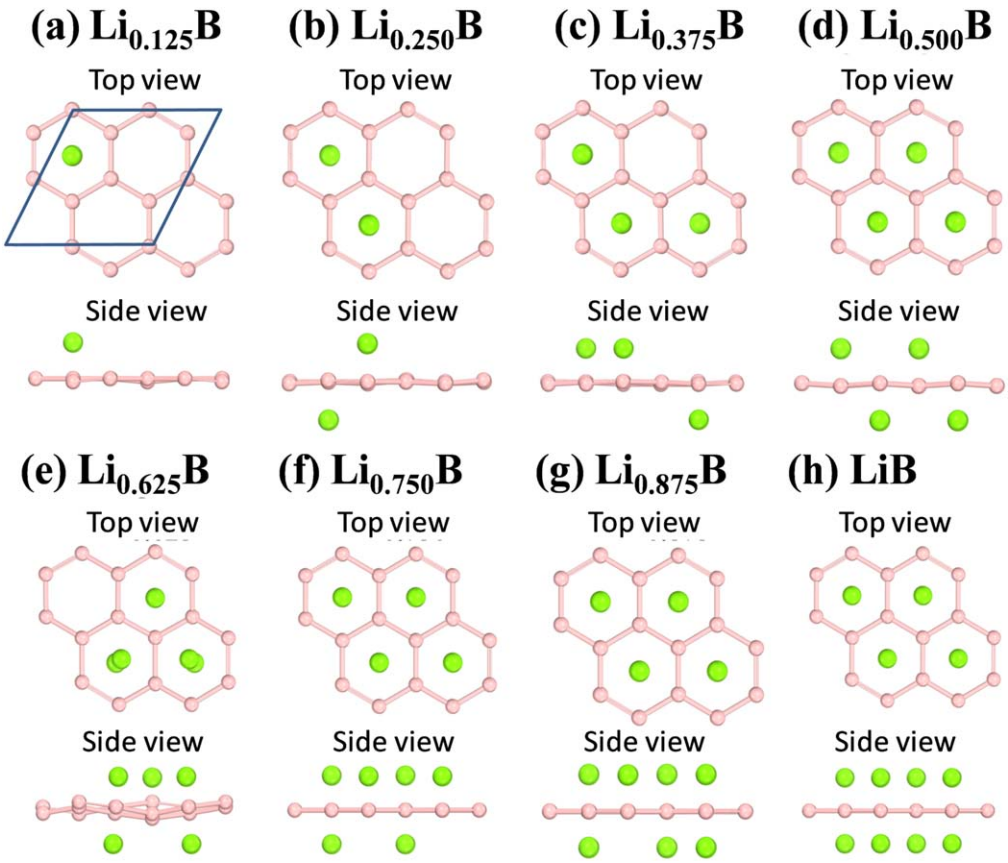

Figure 4. Top and side views of geometry structure of ML (a) $Li_{0.125}B$, (b) $Li_{0.250}B$, (c) $Li_{0.375}B$, (d) $Li_{0.500}B$, (e) $Li_{0.625}B$, (f) $Li_{0.750}B$, (g) $Li_{0.875}B$ and (h) LiB. The pink balls and green balls represent the B and Li atoms, respectively. The rhombus indicates the outline of the 2 × 2 ML *h*-borophene supercells.

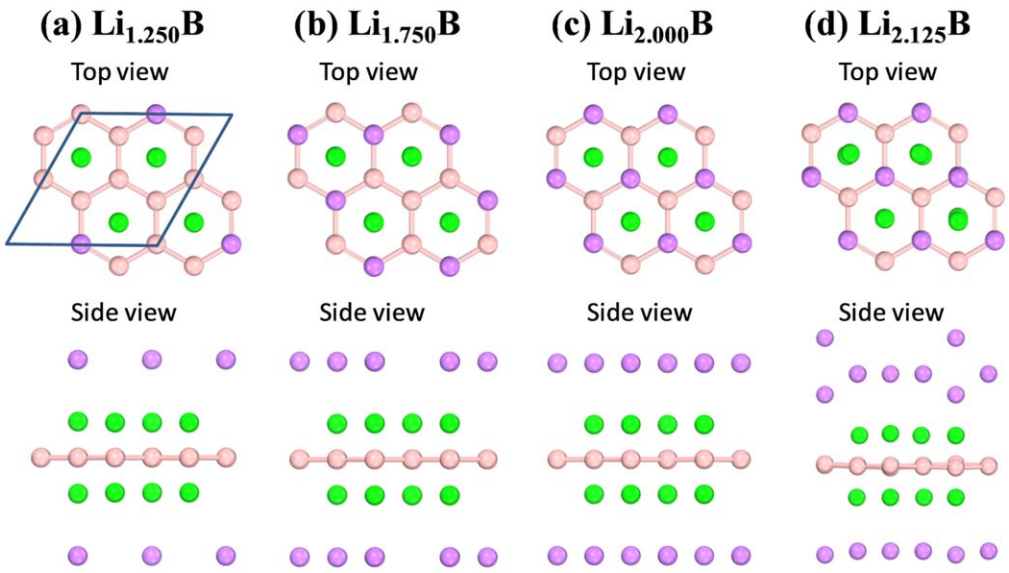

Figure 5. Top and side views of geometry structure of ML (a) $Li_{1.250}B$, (b) $Li_{1.750}B$, (c) $Li_{2.000}B$ and (d) $Li_{2.125}B$. The pink balls, green balls, and purple balls represent the B, the first layer Li and the second layer Li atoms, respectively. The rhombus indicates the outline of the 2 × 2 ML *h*-borophene supercell.

($mAh{\cdot}cm^{-3}$) as the product of the gravimetric capacity C_g ($mAh{\cdot}g^{-1}$) and the effective density of our sample ρ ($g{\cdot}cm^{-3}$).[75] The above maximum theoretical storage capacity C is equivalent to the gravimetric capacity C_g. To estimate the C_v, we should know the effective density ρ first. Here, we adopt the distance between the first top Li/Na layer and the last bottom Li/Na layer of the $Li_{2.125}B$ (10 Å)/$Na_{0.750}B$ (4 Å) system as the effective thickness of the sample. According to the effective thickness, the ρ values of the $Li_{2.125}B$ and the $Na_{0.750}B$ are 1.089 and 2.988 $g{\cdot}cm^{-3}$, respectively. Thus, the C_v values of the $Li_{2.125}B$ and the $Na_{0.750}B$ are 5737 and 5558 $mAh{\cdot}cm^{-3}$, respectively. The C_v values of the $Li_{2.125}B$ and the $Na_{0.750}B$ are much greater than those of graphite (818 $mAh{\cdot}cm^{-3}$), graphynes (1589 $mAh{\cdot}cm^{-3}$) and multilayer α-graphdiyne (2032 $mAh{\cdot}cm^{-3}$) for the LIB.[17]

With the increasing concentration of the Li/Na ions adsorbed on ML *h*-borophene, the binding energy grows up, indicating a possible poor thermodynamic stability of the high concentration systems. Therefore, it is necessary to check the stability of the high adsorption concentration system, such as $Li_{2.125}B$ and $Na_{0.750}B$. After the FPMD simulations, there is no apparent structural deformation in the $Li_{2.125}B$ system at 300 K for 5 ps, as illustrated in Fig. 6b, showing a good thermodynamic stability of the Li adsorbed system. The $Na_{0.75}B$ system at 300 K for 5 ps reveals that a high adsorption concentration of the Na ions induces the deformation of ML *h*-borophene. A puckering of the ML *h*-borophene substrate in the *z* direction with a value of 0.28 Å (as shown in Fig. 6c) reveals that the $Na_{0.75}B$ system is not as stable as the $Li_{2.125}B$ system, but such a small deformation of the ML *h*-borophene substrate in the $Na_{0.75}B$ system should not make a big influence to its systemic stability. So our result of the $Na_{0.750}B$ remains reliable.

Furthermore, we also estimate another important indicator average OCV to reflect the energy density of the LIB/NIB, which is defined as[76]

$$V = -(E_{MnB8} - E_{B8} - nE_M)/(nye) = -E_b/ye \qquad [5]$$

where *y* is the electronic charge of the M (M = Li or Na) ions (here *y* =1). From this equation, the OCV is related to the binding energy E_b and required to be a positive result. A low OCV of the anode materials would be equivalent to a high energy density, while an ultralow OCV for the anode materials would result in the metal plating and the dendrite formation of the adsorbed metal.[48] Figures 3a and 3b show the OCVs for the LIB and NIB as functions of the Li and Na ion concentration, respectively. For the LIB, the OCVs are 1.06, 1.15, 1.05, 1.05, 0.99, 0.96, 0.97 and 0.95 V with the concentration from 0 to 1.000 with a step of 0.125, respectively. The OCVs are 0.50, 0.16, 0.09 and 0.03 V with the concentration of 1.250, 1.750, 2.000 and 2.125, respectively. The overall OCV (numerical average of all the OCVs we calculated) is 0.747 V. For the NIB, the OCVs are 0.68, 0.72, 0.35, 0.21, 0.11 and 0.04 V with the concentration from 0 to 0.75 with a step of 0.125, respectively, and the overall OCV is 0.355 V. Through our calculations, the overall OCVs for the LIBs and NIBs are around the proper voltage

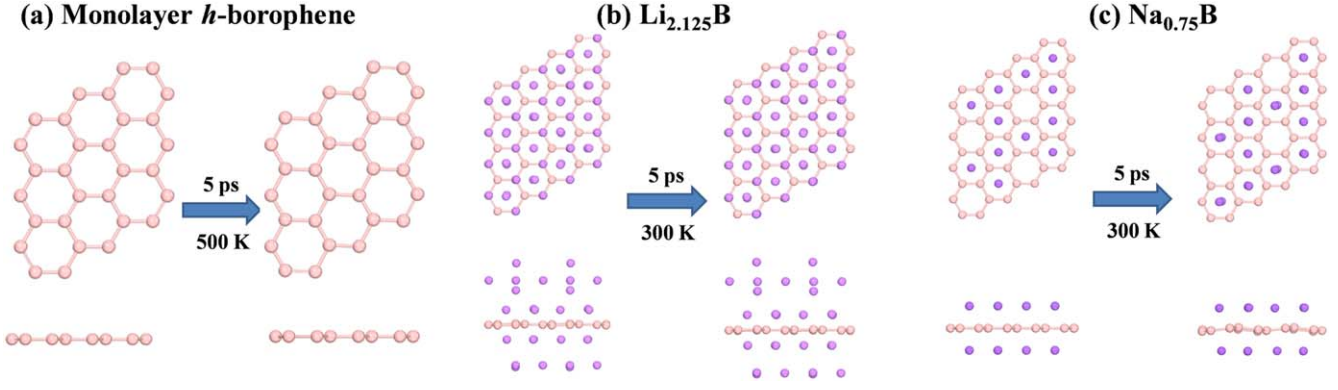

Figure 6. FPMD simulation results to assess the stability of (a) ML *h*-borophene, (b) $Li_{2.125}B$ and (c) $Na_{0.75}B$ system.

value (0.2–1.0 V).[76] Therefore, ML *h*-borophene should be a suitable anode material for both the LIBs and NIBs.

***Electronic properties of the Li/Na ions adsorbed on ML* h-*borophene.*—**Additionally, the good electronic conductivity of the anode materials plays a crucial role in the performance of the LIB and NIB, particularly in the rate capability. Unlike many other 2D materials owning the semiconducting/semi-metallic electronic properties, ML *h*-borophene is naturally metallic, and its PDOS is illustrated in Fig. 7a. There is a Dirac state at the energy of 3.33 eV, but the Dirac state is far away from the Fermi level of ML *h*-borophene, and such an electronic state makes no influence on the metallic property of ML *h*-borophene and is in good agreement with the previous experiment.[43] Hence, it is expected that the pristine ML *h*-borophene has enough electronic states to transfer the electrons as an anode material. The PDOS of the most stable Li/Na ion adsorption configurations of 2×2 ML *h*-borophene at every concentration are also calculated because the insertion of the Li/Na ions into the anode materials could influence the electronic property of the pristine ML *h*-borophene substrate. To further illustrate the electronic conductivity of ML *h*-borophene with the adsorbed metal ions, the PDOS of the Li ions adsorption configurations of ML *h*-borophene are shown in Figs. 7b–7i and Figs. 8a–8d, and the PDOS of the Na ions adsorption configurations of ML *h*-borophene are shown in Figs. S2a–S2f. As we can see, the electronic structure of the ML *h*-borophene undergoes some changes upon the Li/Na ion adsorption as a consequence of electron transfer from the Li/Na atoms to ML *h*-borophene. However, we find that the PDOS profiles near the Fermi level are all non-zero, and intrinsically metallic property of ML *h*-borophene remains unchanged during the whole process, and an excellent electronic conductivity of ML *h*-borophene is maintained. It suggests that ML *h*-borophene keep its good electrical conductivity characteristics after the adsorption process of the Li/Na ions, which paves the way for its application as the anode materials for the LIB/NIB.

***Crystal structures and adsorption ability of a Li/Na atom on multiple layer* h-*borophene.*—**To advance our study, we model the bilayer (BL), trilayer (TL) and four-layer (FL) *h*-borophene adsorption system as the representative of the multiple layer system. To confirm the stability of the multiple layer borophene system, we defined average formation energy (E_{form}) as $E_{form} = E_B - E_{tot}$, where E_B is the energy of an isolated B atom, and E_{tot} is the total energy per atom of multiple layer borophene. We optimized the geometry structures of the two *h*-borophene layers stacked together in either AA or AB arrangement and obtain the average formation energy of the AA (5.76 eV atom^{-1}) and AB (5.94 eV atom^{-1}) stacking system. The higher energy structure corresponding to the AB stacking is with a lattice constant of 3.0 Å, a puckering (Δ) of 0.16 Å within each layer and an interlayer distance of 1.46 Å as shown in Fig. S3a. Similarly, we check the stability of the AA and AB arrangement of the TL and FL *h*-borophene system. The average formation energies of the TL AA and AB stacking systems are 5.85 and 6.09 eV atom^{-1}, respectively. The more stable TL AB stacking

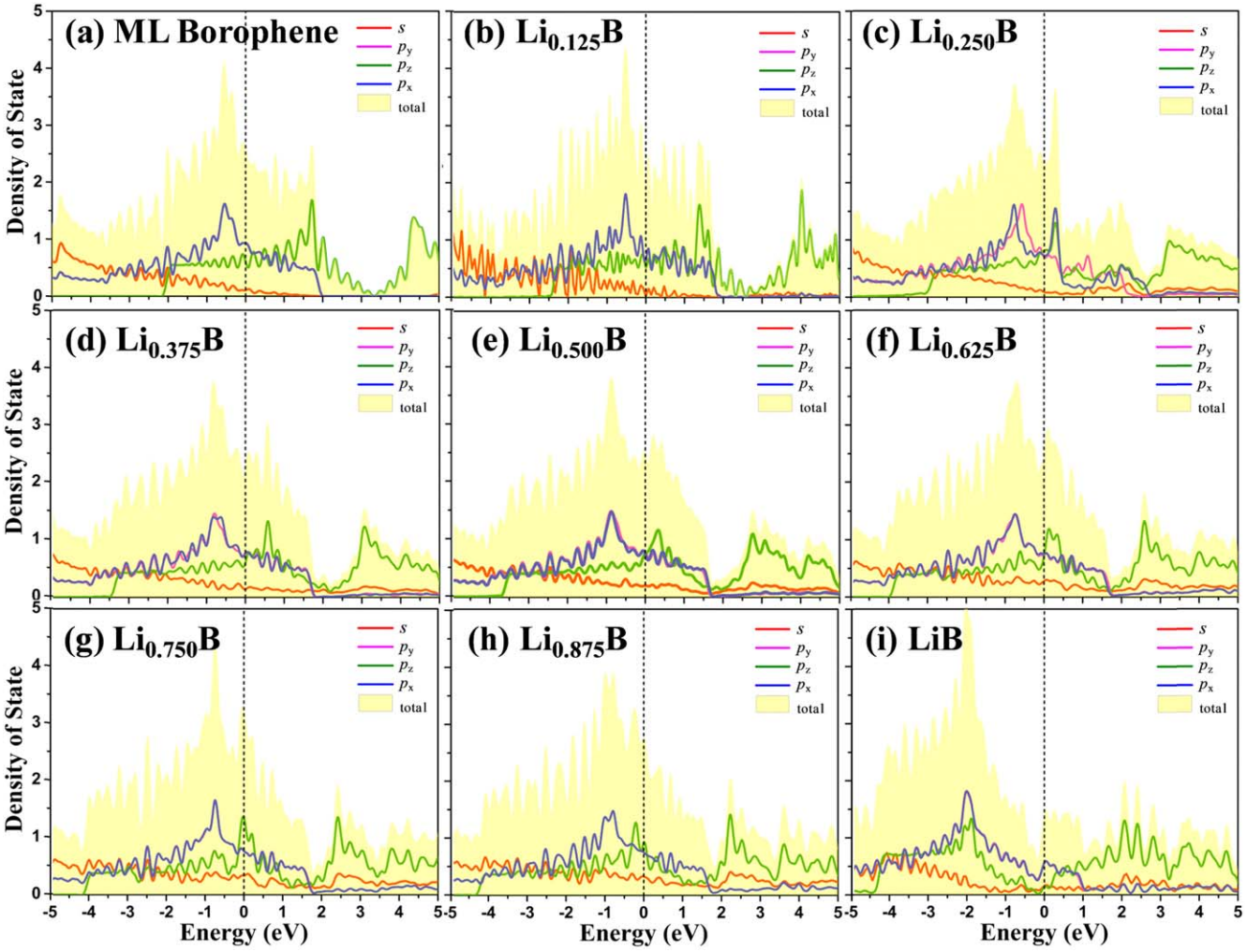

Figure 7. Projected density of states (PDOS) of ML (a) pristine *h*-borophene, (b) $Li_{0.125}B$, (c) $Li_{0.250}B$, (d) $Li_{0.375}B$, (e) $Li_{0.500}B$, (f) $Li_{0.625}B$, (j) $Li_{0.750}B$, (h) $Li_{0.875}B$ and (i) LiB. The black dash lines represent the Fermi level.

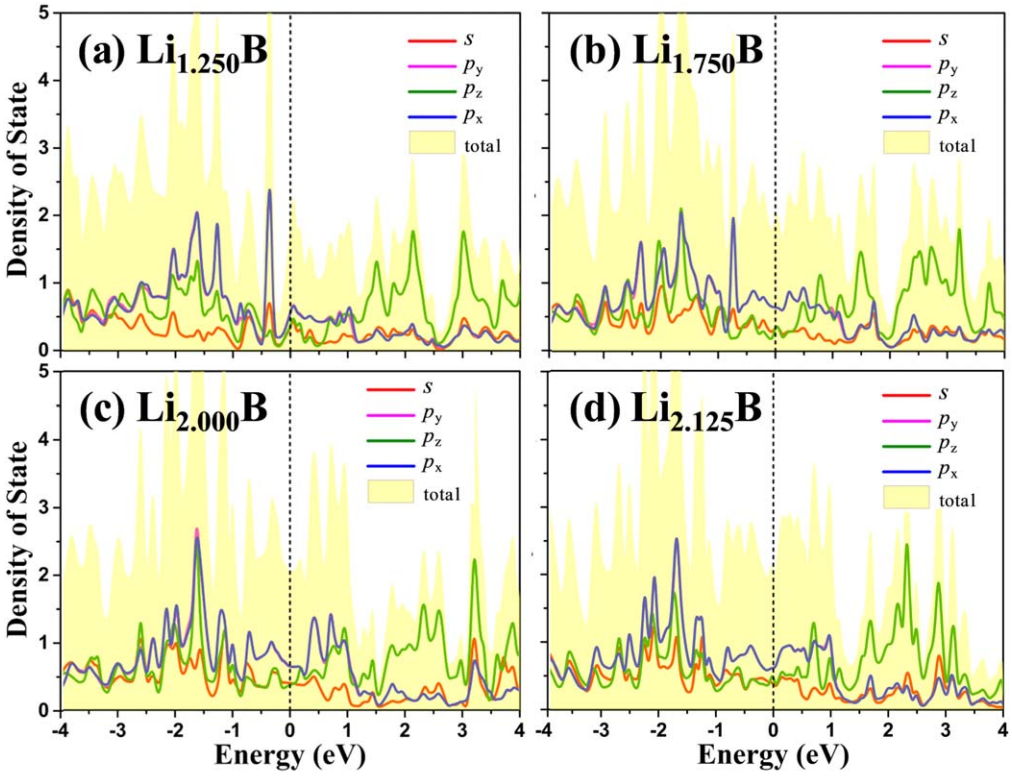

Figure 8. Projected density of states (PDOS) of ML (a) $Li_{1.250}B$, (b) $Li_{1.750}B$, (c) $Li_{2.000}B$ and (d) $Li_{2.125}B$. The black dash lines represent the Fermi level.

h-borophene has a lattice constant of 3.0 Å and an interlayer distance of 1.60 Å as given in Fig. S3b. For the FL, the average formation energies of the AA and AB stacking systems are 5.84 and 6.19 eV $atom^{-1}$, respectively. The FL AB stacking *h*-borophene owns a lattice constant of 3.0 Å, a puckering (Δ) of 0.13 Å within the first/fourth layer, a puckering of 0.25 Å within the second/third layer, a distance between the first (third) to the second (fourth) layer of 1.56 Å and a distance between the second to the third layer of 1.72 Å as shown in Fig. S3c. In all the AB staking systems, the even layer of multiple layer *h*-borophene is shifted 0.89 Å along the long diagonal axis relative to the odd layer of multiple layer *h*-borophene. Comparing the average formation energy of ML (5.29 eV $atom^{-1}$), BL (5.94 eV $atom^{-1}$), TL (6.09 eV $atom^{-1}$) and FL (6.19 eV $atom^{-1}$) *h*-borophene, the related *h*-borophene system become more and more stable with the increasing of the number of *h*-borophene layers. We use these AB configurations to study the adsorption interaction of the Li/Na atoms with multiple layer *h*-borophene.

Before studying the Li/Na atom adsorption ability of multiple layer *h*-borophene, we should know the most stable adsorption sites to evaluate the adsorption ability of an isolated Li/Na atom on the multiple layer *h*-borophene surface. In order to make our adsorption ability results of ML *h*-borophene comparable to that of multiple layer *h*-borophene, we still use a 2 × 2 *h*-borophene supercell with one Li/Na atom adsorbed on to investigate the adsorption properties. Considering the symmetry of the multiple layer *h*-borophene lattice, there are seven typical types of possibly the most stable adsorption sites. We mark these typical adsorption sites from 1 to 7 in Figs. S3a–S3c, and the adsorption sites 1 to 6 are the sites located on the surface of the multiple layer *h*-borophene system, while the site 7 is the interlayer adsorption site. After geometric optimization, all the Li/Na atoms adsorbed on the interlayer site 7 automatically shift to the surface of the multiple layer *h*-borophene system, indicating a Li/Na atom surface adsorption characteristic of the *h*-borophene system.

Then, we will focus on the stability of the surface adsorption site 1 to 6 to find the most stable position of a Li/Na atom adsorbed on the BL, TL and FL *h*-borophene. Calculating the adsorption energy is a good way to reflect the stability and study the adsorption ability of the multiple layer *h*-borophene system. In order to calculate the adsorption energy in the BL system, we use Eq. 1 and replace E_{MxB8} and E_{B8} with the total energy of the 2 × 2 BL/TL/FL *h*-borophene adsorbed by the metal atoms and pristine 2 × 2 BL/TL/FL *h*-borophene, respectively. The "binding" and "adsorption" are used interchangeably in our cases. After the optimization of BL h-borophene with a Li atom adsorbed on the site 1, 2, 3 and 4, the isolated Li atom of the four systems will stay on or shift to the site 1 with the adsorption energy of −2.11 eV $atom^{-1}$. For the BL *h*-borophene with a Li atom adsorbed on the site 5 and 6, the isolated Li atom of the two systems will move to the middle of the site 1 and 6 with the adsorption energy of −2.68 eV $atom^{-1}$, and this position is the most stable adsorption site of the Li atom-BL *h*-borophene system as illustrated in Fig. S4a. Optimized the BL *h*-borophene with a Na atom adsorbed on the site 1 and 6 systems, the isolated Na atom of the two systems will stay on or shift to the site 1 with the adsorption energy of −0.74 eV $atom^{-1}$. The Na atom adsorbed on the site 4 of the BL *h*-borophene surface stay on its initial position, and the adsorption energy is −1.20 eV $atom^{-1}$. The BL *h*-borophene with a Na atom adsorbed on the site 2, 3 and 5, the isolated Na atom of the three systems will move to the position shown in Fig. S4d, and the adsorption energy of this system is −1.25 eV $atom^{-1}$.

In the TL system, the isolated Li or Na adsorbed on the site 1, 2, 3, 4, 5 and 6 will stay on or move to the site 1, and the structure of the most stable a Li atom-TL *h*-borophene and a Na atom-TL *h*-borophene are illustrated in Figs. S4b and S4e, respective, and the adsorption energy is −1.68 eV $atom^{-1}$ for the Li atom adsorption system and −1.06 eV $atom^{-1}$ for the Na atom adsorption system. The adsorption situation in the FL system is quite similar to that in the TL system. The isolated Li adsorbed on the site 1, 2, 3, 4, 5 and 6 of the FL *h*-borophene system will stay on or shift to the site 1 (as shown in Fig. S4c) with the adsorption energy of −1.36 eV $atom^{-1}$.

The isolated Na adsorbed on the site 3 of the FL *h*-borophene system will stay on its initial position with the adsorption energy of -0.24 eV atom^{-1}, and the Na atom adsorbed on the other sites will stay on or move to the site 1 (as illustrated in Fig. S4f) with the adsorption energy of -0.75 eV atom^{-1}. Finally, we summarize the structural parameters and the adsorption energy of a Li/Na adsorbed on ML/BL/TL/FL *h*-borophene in Table SII. By comparing the adsorption energy of the Li/Na atom-ML/BL/TL/FL *h*-borophene system, we find that the adsorption energy increases with the number of the *h*-borophene layers, and when the number of layers is increased to enough number, the adsorption energy of the multiple layer *h*-borophene system will be very close to that of ML system due to the surface adsorption characteristic of the Li/Na atom adsorption system.

Comparison with other two-dimensional anode materials.—Up to now, the indicators of ML *h*-borophene as an anode for the LIB and NIB perform well. To further demonstrate its significant potential to be applied in the LIB and NIB, we compare the diffusion barrier, maximum theoretical storage capacity and OCV of the ML *h*-borophene-Li/Na ions storage system with those of other ML 2D materials-Li/Na ions storage system. At first, we compare ML *h*-borophene to other ML borophene compatriots. As we mentioned before, the experiments yield six types of borophene with different vacancies, and three of the synthesized borophene (2-*Pmm*, β_{12} and χ_3 borophene) and one theoretical semiconducting β_{1S} borophene have been calculated as the anode materials of the LIB and NIB, thus we totally list five types of borophene as the anode materials for the LIB and NIB in Table II.[46–51,77] For the LIB, the diffusion barrier of *h*-borophene (0.53 eV) is two orders of magnitude higher than that of 2-*Pmm* borophene (2.6 $\sim$ 25 meV) and slightly larger than that of β_{1S} borophene (0.40 eV), but it is still smaller than that of χ_3 (0.60 $\sim$ 0.63 eV) and β_{12} (0.61 $\sim$ 0.66 eV) borophene. We can see that the maximum theoretical storage capacities of the Li ions are in the order of β_{1S} (1240 mAh·g^{-1}) < χ_3 (1240 $\sim$ 1487 mAh·g^{-1}) < β_{12} (1983/1984 mAh·g^{-1}) < 2-*Pmm* (1239 $\sim$ 3306 mAh·g^{-1}) < *h*-borophene (5268 mAh·g^{-1}), and the capacity of ML *h*-borophene is the largest one among all the compared ML borophene.[46–51,77] The OCVs of Li-storage of five types of ML borophene are comparable to the proper OCV for the anode in the range of 0.747 $\sim$ 2.37 V, and the OCV of ML *h*-borophene is the lowest one.

Figure 9a shows the comparison of the diffusion barrier vs the maximum storage capacity of the LIB between ML *h*-borophene and other thirty kinds of ML 2D materials, and the 2D materials with a maximum storage capacity below 1000 mAh·g^{-1} are zoomed in Fig. S5a. In order to obtain a suitable anode material, we only discuss the ML 2D material whose OCV is less than 2.0 V and whose capacity is larger than the theoretical one of graphite (372 mAh·g^{-1}). To be noted, the capacity of ML *h*-borophene (5268 mAh·g^{-1}) can be 8 to 12 times higher than those of ML black phosphorene (432.79 mAh·g^{-1}),[78] MoN_2 (432 mAh·g^{-1}),[31] TiN_2 (484 mAh·g^{-1}),[79,80] borophane (504 mAh·g^{-1}),[81] VS_2 (466 mAh·g^{-1}),[27] GaS (526.74 mAh·g^{-1}),[34] Nb_2C (542 mAh·g^{-1}),[23] Mo_2C (526 mAh·g^{-1})[24] and V_3C_2 (606.42 mAh·g^{-1});[21] five to seven times as high as those of graphene (744 mAh·g^{-1}),[14] silicene (954 mAh·g^{-1}),[15,16] blue phosphorene (865 mAh·g^{-1}),[20] C_3B (714 mAh·g^{-1})[82] and V_2C (941 mAh·g^{-1});[83] twice to five times larger than those of ML triphenylene-graphdiyne (1097 mAh·g^{-1}),[84] B_3S (1662 mAh·g^{-1}),[32] NiC_3 (1698 mAh·g^{-1}),[22] Mg_3N_2 (1858 mAh·g^{-1}),[29] P-triphenylene-graphdiyne (1979 mAh·g^{-1}),[84] N-triphenylene-graphdiyne (2664 mAh·g^{-1})[84] and pentagonal-BN_2 (2071 mAh·g^{-1}).[85] The capacity of ML *h*-borophene is one and a half times larger than that of ML C_2N (2939 mAh·g^{-1}).[86,87] It is worth mentioning that the capacity of ML *h*-borophene (5268 mAh·g^{-1}) is more than 1000 mAh·g^{-1} larger than that of ML graphdiyne (4259 mAh·g^{-1}),[17] and we can conclude that the capacity of ML *h*-borophene is the highest one among all the reported possible anode 2D material after a systematic comparison.

For the Na-storage, both the diffusion barrier (0.17 eV) and OCV (0.355 V) of *h*-borophene is apparently lower than those of any other types of borophene except for 2-*Pmm* borophene with the diffusion barrier of 2 $\sim$ 3 meV and the OCV of 0.287 $\sim$ 1.700 V.[46–50] Although the capacity of *h*-borophene for the Na ions (1860 mAh·g^{-1}) is lower than that of β_{12} (1984 mAh·g^{-1}) and 2-*Pmm* (2341 mAh·g^{-1}) borophene,[46,51] it is larger than those of β_{1S} (1240 mAh·g^{-1}) and χ_3 (1240 mAh·g^{-1}) borophene and remains five times higher than that of commercial graphite (372 mAh·g^{-1}) and over 53 times as high as that of theoretical graphite-based NIB.[54] As we expected, the storage capacity of ML *h*-borophene as an anode of the LIB is ultra high due to its high density of the adsorption sites and lightweight. The performance of ML *h*-borophene as an anode of the NIB is not as good as that of the LIB because the radius of the Na ion is longer than that of the Li ion resulting in a weaker adsorption ability of the Na ion on ML *h*-borophene.

Figure 9b shows the comparison of the diffusion barrier of the NIB vs the maximum storage capacity of the NIB between ML *h*-borophene and other 27 kinds of ML 2D materials, and the materials with a maximum storage capacity below 550 mAh·g^{-1} are zoomed

Table II. Summary of the theoretical capacity (mAh·g^{-1}), diffusion barrier (eV), and open-circuit voltage (V) of five phases of ML borophene (2-*Pmm*, β_{12}, χ_3, β_{1S}, *h*) as the anode for the LIB and NIB.

Metal ion type	Borophene structure	Theoretical capacity (mAh·g^{-1})	Diffusion barrier (meV)	OCV (V)	References
Li	2-*Pmm*	1720	25	—	47
		1864	9	1.17	48
		1239	7	1.11	49
		1860	2.6	1.12	50
		3306	10.53	2.37	51
	β_{12}	1984	660	1.26	46
		1983	610	1.42	48
	χ_3	1240	600	1.09	46
		1487	628	1.22	48
	β_{1S}	1240	400	1.11	77
	h	5268	540	0.747	This work
Na	2-*Pmm*	1380	3	—	47
		—	2	0.287	49
		2341	2.3	1.7	51
	β_{12}	1984	330	0.88	46
	χ_3	1240	340	0.78	46
	β_{1S}	1240	300	0.88	77
	h	1860	170	0.355	This work

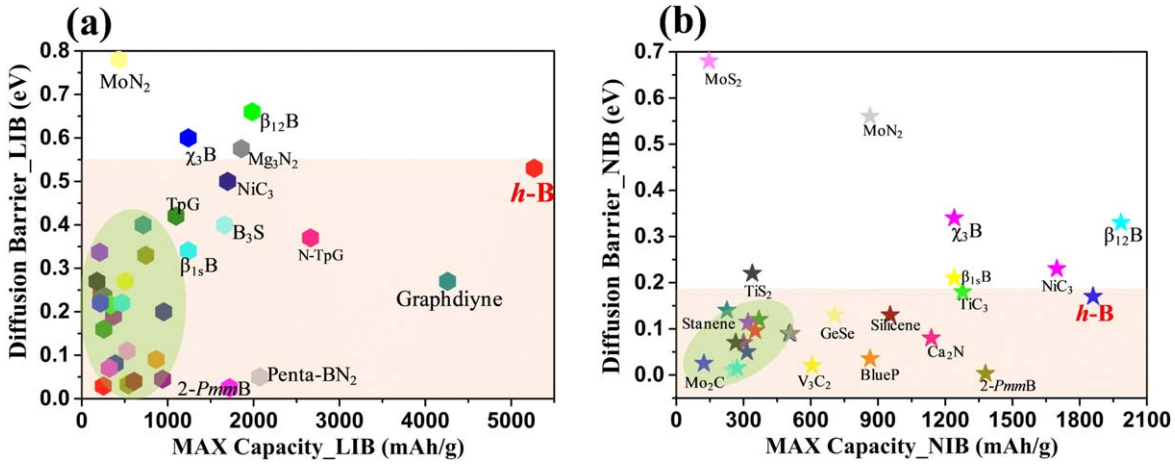

Figure 9. DFT calculated diffuse barriers and the maximum storage capacities of ML *h*-borophene and other typical ML 2D anode materials for (a) LIB and (b) NIB. The ML 2D materials covered with the purple shadows have lower diffusion barriers and smaller maximum storage capacity than ML *h*-borophene. Some data are taken from the literatures.[13–34,78,81–85,88,89,90–93]

in Fig. S5b. The capacity of ML *h*-borophene anode of the NIB (1860 mAh·g^{-1}) is not as high as that of β_{12} and 2-*Pmm* borophene anode of the NIB, but it is still superior to those of the majority ML 2D material as the anode of the NIB. It is twice to 13 times higher than those of ML borophane (504 mAh·g^{-1}),[81] TiN_2 (484 mAh·g^{-1}),[79,80] graphene (300 mAh·g^{-1}),[13,14] silicene (954 mAh·g^{-1}),[15,16] germanene (369 mAh·g^{-1}),[16,88] stanene (226 mAh·g^{-1}),[16] black phosphorene (315 mAh·g^{-1}),[18,19] antimonene (320 mAh·g^{-1}),[89] Mo_2B_2 (251 mAh·g^{-1}),[94] Sr_2N (283 mAh·g^{-1}),[30] MoN_2 (864 mAh·g^{-1}),[31] Ca_2N (1138),[30] MoS_2 (146 mAh·g^{-1}),[25,26] $CoTe_2$ (150 mAh·g^{-1}),[95] $NiTe_2$ (150 mAh·g^{-1}),[95] ZrS_2 (270 mAh·g^{-1}),[95] NbS_2 (265 mAh·g^{-1}),[95] CrS_2 (325 mAh·g^{-1}),[95] VS_2 (330 mAh·g^{-1}),[95] TiS_2 (339 mAh·g^{-1}),[95] Mo_2C (123 mAh·g^{-1}),[24] Nb_2C (271 mAh·g^{-1}),[23] Ti_3C_2 (351.8 mAh·g^{-1}),[90] V_3C_2 (606.42 mAh·g^{-1})[21] and GeS_2 (512 mAh·g^{-1}).[91] The capacity of ML *h*-borophene as an anode of the NIB is comparable to those of ML TiC_3 (1278 mAh·g^{-1})[73] and NiC_3 (1698 mAh·g^{-1}),[22] but the diffusion barriers of ML TiC_3 (0.18 eV)[73] and NiC_3 (0.23 eV)[22] for the NIB are higher than that of ML *h*-borophene (0.17 eV). Although the capacity of ML C_2N (2469 mAh·g^{-1}) is larger than that of ML *h*-borophene, the diffusion barrier of ML C_2N (>2.8 eV) is far greater than that of ML *h*-borophene.[86,87] Taken together, ML *h*-borophene is a promising candidate as the anode material for the NIB.

Conclusions

We investigate the LIB and NIB performance of 2 × 2 ML *h*-borophene as the anode electrodes by studying the adsorption ability, transition states, geometry and electronic structures using first-principles DFT calculations. ML *h*-borophene as the anode materials of the LIB and NIB has good electrical conductivity before and after the adsorption process, proper average OCVs of 0.747 V for the LIB and 0.355 V for the NIB, and small structural distortions. In addition, Na ion has a low diffusion barrier with a height of 0.17 eV on the ML *h*-borophene surface, and the maximum concentration $Na_{0.75}B$ corresponds to a high capacity of 1860 mAh·g^{-1}. Although the diffusion barrier of the Li ion (0.53 eV) is not as low as that of the Na ion, it is still comparable to those of some well-known anode materials, such as TiO_2-based polymorphs (~0.5 eV). As a highly attractive finding, ML *h*-borophene is predicted to yield ultra-high storage capacities of 5268 mAh·g^{-1} for the Li ions. Comparing the DFT results pertaining to the LIB performance of more than thirty reported ML 2D anode materials with that of ML *h*-borophene, we conclude that the theoretical maximum storage capacity of ML *h*-borophene is the highest one among all the studied ML 2D materials. Our study highly supports that ML *h*-borophene is a promising anode material for both the LIBs and NIBs with good conductivity, high energy density, good recharge rate capacity and high storage capacity, especially an extremely high storage capacity for the LIB.

Acknowledgments

This work was supported by the Ministry of Science and Technology of China (no. 2016YFB0700600 (National Materials Genome Project) and 2017YFA206303), the National Natural Science Foundation of China (nos. 11674005, 91964101, and 11664026) and the High Performance Computing Platform of Peking University.

ORCID

Jingzhen Li https://orcid.org/0000-0002-2090-0079

References

1. L. Lu, X. Han, J. Li, J. Hua, and M. Ouyang, "A review on the key issues for lithium-ion battery management in electric vehicles." *J. Power Sources*, **226**, 272 (2013).
2. N. Nitta, F. Wu, J. T. Lee, and G. Yushin, "Li-ion battery materials: present and future." *Mater. Today*, **18**, 252 (2015).
3. J. B. Goodenough and K. S. Park, "The Li-ion rechargeable battery: a perspective." *J. Am. Chem. Soc.*, **135**, 1167 (2013).
4. J.-M. Tarascon and M. Armand, "Issues and challenges facing rechargeable lithium batteries." *Nature*, **414**, 359 (2001).
5. N. Yabuuchi, K. Kubota, M. Dahbi, and S. Komaba, "Research development on sodium-ion batteries." *Chem. Rev.*, **114**, 11636 (2014).
6. M. D. Slater, D. Kim, E. Lee, and C. S. Johnson, "Sodium-Ion batteries." *Adv. Funct. Mater.*, **23**, 947 (2013).
7. S.-W. Kim, D.-H. Seo, X. Ma, G. Ceder, and K. Kang, "Electrode materials for rechargeable sodium-ion batteries: potential alternatives to current lithium-ion batteries." *Adv. Energy Mater.*, **2**, 710 (2012).
8. B. Scrosati and J. Garche, "Lithium batteries: status, prospects and future." *J. Power Sources*, **195**, 2419 (2010).
9. Y. Zhao, X. Li, B. Yan, D. Li, S. Lawes, and X. Sun, "Significant impact of 2D graphene nanosheets on large volume change tin-based anodes in lithium-ion batteries: a review." *J. Power Sources*, **274**, 869 (2015).
10. L. Shi and T. Zhao, "Recent advances in inorganic 2D materials and their applications in lithium and sodium batteries." *J. Mater. Chem. A*, **5**, 3735 (2017).
11. J. Liu and X. W. Liu, "Two-dimensional nanoarchitectures for lithium storage." *Adv. Mater.*, **24**, 4097 (2012).
12. X. Zhang, L. Hou, A. Ciesielski, and P. Samorì, "2D materials beyond graphene for high-performance energy storage applications." *Adv. Energy Mater.*, **6**, 16006711 (2016).
13. D. H. Wu, Y. F. Li, and Z. Zhou, "First-principles studies on doped graphene as anode materials in lithium-ion batteries." *Theor. Chem. Acc.*, **130**, 209 (2011).
14. R. Raccichini, A. Varzi, S. Passerini, and B. Scrosati, "The role of graphene for electrochemical energy storage." *Nat. Mater.*, **14**, 271 (2015).
15. G. A. Tritsaris, E. Kaxiras, S. Meng, and E. Wang, "Adsorption and diffusion of lithium on layered silicon for Li-ion storage." *Nano Lett.*, **13**, 2258 (2013).
16. B. Mortazavia, A. Dianatb, G. Cunibertib, and T. Rabczuk, "Application of silicene, germanene and stanene for Na or Li ion storage: a theoretical investigation." *Electrochim. Acta*, **213**, 865 (2016).

17. B. Jang, J. Koo, M. Park, H. Lee, J. Nam, Y. Kwon, and H. Lee, "Graphdiyne as a high-capacity lithium ion battery anode material." *Appl. Phys. Lett.*, **103**, 2639041 (2013).
18. W. Li, Y. Yang, G. Zhang, and Y. W. Zhang, "Ultrafast and directional diffusion of lithium in phosphorene for high-performance lithium-ion battery." *Nano Lett.*, **15**, 1691 (2015).
19. A. Sibari, Z. Kerrami, A. Kara, M. Hamedoun, A. Benyoussef, O. Mounkachi, and M. Benaissa, "Adsorption and diffusion on a phosphorene monolayer: a DFT study." *J. Solid State Electrochem.*, **22**, 11 (2017).
20. G. Barik and S. Pal, "Energy gap-modulated blue phosphorene as flexible anodes for lithium- and sodium-ion batteries." *J. Phys. Chem. C*, **123**, 2808 (2019).
21. K. Fan, Y. Ying, X. Li, X. Luo, and H. Huang, "Theoretical investigation of V_3C_2 MXene as prospective high-capacity anode material for metal-ion (Li, Na, K, and Ca) batteries." *J. Phys. Chem. C*, **123**, 18207 (2019).
22. C. Zhu, X. Qu, M. Zhang, J. Wang, Q. Li, Y. Geng, Y. Ma, and Z. Su, "Planar NiC_3 as a reversible anode material with high storage capacity for lithium-ion and sodium-ion batteries." *J. Mater. Chem. A*, **7**, 13356 (2019).
23. J. Hu, B. Xu, C. Ouyang, Y. Zhang, and S. A. Yang, "Investigations on Nb_2C monolayer as promising anode material for Li or non-Li ion batteries from first-principles calculations." *RSC Adv.*, **6**, 27467 (2016).
24. Q. Sun, Y. Dai, Y. Ma, T. Jing, W. Wei, and B. Huang, "Ab initio prediction and characterization of Mo_2C monolayer as anodes for lithium-ion and sodium-ion batteries." *J. Phys. Chem. Lett.*, **7**, 937 (2016).
25. M. Mortazavi, C. Wang, J. Deng, V. B. Shenoy, and N. V. Medhekar, "Ab initio characterization of layered MoS_2 as anode for sodium-ion batteries." *J. Power Sources*, **268**, 279 (2014).
26. Y. Li, D. Wu, Z. Zhou, C. R. Cabrera, and Z. Chen, "Enhanced Li adsorption and diffusion on MoS_2 zigzag nanoribbons by edge effects: a computational study." *J. Phys. Chem. Lett.*, **3**, 2221 (2012).
27. Y. Jing, Z. Zhou, C. R. Cabrera, and Z. Chen, "Metallic VS_2 monolayer: a promising 2D anode material for lithium ion batteries." *J. Phys. Chem. C*, **117**, 25409 (2013).
28. X. Xie, M. Mao, S. Qi, and J. Ma, "ReS_2-based electrode materials for alkali-metal ion batteries." *CrystEngComm*, **21**, 3755 (2019).
29. L. Xiong, J. Hu, S. Yu, M. Wu, B. Xu, and C. Ouyang, "Density functional theory prediction of Mg_3N_2 as a high-performance anode material for Li-ion batteries." *Phys. Chem. Chem. Phys.*, **21**, 7053 (2019).
30. S. Deng, L. Wang, T. Hou, and Y. Li, "Two-dimensional MnO_2 as a better cathode material for lithium ion batteries." *J. Phys. Chem. C*, **119**, 28783 (2015).
31. X. Zhang, Z. Yu, S.-S. Wang, S. Guan, H. Y. Yang, Y. Yao, and S. A. Yang, "Theoretical prediction of MoN_2 monolayer as a high capacity electrode material for metal ion batteries." *J. Mater. Chem. A*, **4**, 15224 (2016).
32. S. Jana, S. Thomas, C. H. Lee, B. Jun, and S. U. Lee, "B_3S monolayer: prediction of a high-performance anode material for lithium-ion batteries." *J. Mater. Chem. A*, **7**, 12706 (2019).
33. A. Sannyal, Z. Zhang, X. Gao, and J. Jang, "Two-dimensional sheet of germanium selenide as an anode material for sodium and potassium ion batteries: first-principles simulation study." *Comput. Mater. Sci.*, **154**, 204 (2018).
34. X. Zhang et al., "Monolayer GaS with high ion mobility and capacity as a promising anode battery material." *J. Mater. Chem. A*, **7**, 14042 (2019).
35. J. He, K. Bao, W. Cui, J. Yu, C. Huang, X. Shen, Z. Cui, and N. Wang, "Construction of large-area uniform graphdiyne film for high-performance lithium-ion batteries." *Chem. Eur. J.*, **24**, 1187 (2018).
36. T. Zhou, W. K. Pang, C. Zhang, J. Yang, Z. Chen, H. K. Liu, and Z. Guo, "Enhanced sodium-ion battery performance by structural phase transition from two-dimensional hexagonal-SnS_2 to orthorhombic-SnS." *ACS Nano*, **8**, 8323 (2014).
37. E. J. Yoo, J. Kim, E. Hosono, H.- S. Zhou, T. Kudo, and I. Honma, "Large reversible Li storage of graphene nanosheet families for use in rechargeable lithium ion batteries." *Nano Lett.*, **8**, 2277 (2008).
38. X. Wu, J. Dai, Y. Zhao, Z. Zhuo, J. Yang, and X. C. Zen, "Two-dimensional boron monolayer sheets." *ACS Nano*, **6**, 7443 (2012).
39. Y. Liu, E. S. Penev, and B. I. Yakobson, "Probing the synthesis of two-dimensional boron by first-principles computations." *Angew. Chem. Int. Ed. Engl.*, **52**, 3156 (2013).
40. H. Liu, J. Gao, and J. Zhao, "From boron cluster to two-dimensional boron sheet on Cu(111) surface: growth mechanism and hole formation." *Sci. Rep.*, **3**, 32381 (2013).
41. A. J. Mannix et al., "Synthesis of borophenes: anisotropic, two-dimensional boron polymorphs." *Science*, **350**, 1513 (2015).
42. B. Feng, J. Zhang, Q. Zhong, W. Li, S. Li, H. Li, P. Cheng, S. Meng, L. Chen, and K. Wu, "Experimental realization of two-dimensional boron sheets." *Nat. Chem.*, **8**, 563 (2016).
43. W. Li, L. Kong, C. Chen, J. Gou, S. Sheng, W. Zhang, H. Li, L. Chen, P. Cheng, and K. Wu, "Experimental realization of honeycomb borophene." *Sci. Bull.*, **63**, 282 (2018).
44. R. Wu, I. K. Drozdov, S. Eltinge, P. Zahl, S. Ismail-Beigi, I. Bozovic, and A. Gozar, "Large-area single-crystal sheets of borophene on Cu(111) surfaces." *Nat. Nanotechnol.*, **14**, 44 (2019).
45. B. Kiraly, X. Liu, L. Wang, Z. Zhang, A. J. Mannix, B. L. Fisher, B. I. Yakobson, M. C. Hersam, and N. P. Guisinger, "Borophene synthesis on Au(111)." *ACS Nano*, **13**, 3816 (2019).
46. X. Zhang, J. Hu, Y. Cheng, H. Y. Yang, Y. Yao, and S. A. Yang, "Borophene as an extremely high capacity electrode material for Li-ion and Na-ion batteries." *Nanoscale*, **8**, 15340 (2016).
47. B. Mortazavi, A. Dianat, O. Rahaman, G. Cuniberti, and T. Rabczuk, "Borophene as an anode material for Ca, Mg, Na or Li ion storage: a first-principle study." *J. Power Sources*, **329**, 456 (2016).
48. M. Boroun, S. Abdolhosseini, and M. Pourfath, "Separated and intermixed phases of borophene as anode material for lithium-Ion batteries." *J. Phys. D: Appl. Phys.*, **52**, 2455011 (2019).
49. Y. Zhang, Z. F. Wu, P. F. Gao, S. L. Zhang, and Y. H. Wen, "Could borophene be used as a promising anode material for high-performance lithium ion battery?" *ACS Appl. Mater. Interfaces*, **8**, 22175 (2016).
50. H. R. Jiang, Z. Lu, M. C. Wu, F. Ciucci, and T. S. Zhao, "Borophene: a promising anode material offering high specific capacity and high rate capability for lithium-ion batteries." *Nano Energy*, **23**, 97 (2016).
51. D. Rao, L. Zhang, Z. Meng, X. Zhang, Y. Wang, G. Qiao, X. Shen, H. Xia, J. Liu, and R. Lu, "Ultrahigh energy storage and ultrafast ion diffusion in borophene-based anodes for rechargeable metal ion batteries." *J. Mater. Chem. A*, **5**, 2328 (2017).
52. H. Li, L. Jing, W. Liu, J. Lin, R. Y. Tay, S. H. Tsang, and E. H. T. Teo, "Scalable production of few-layer boron sheets by liquid-phase exfoliation and their superior supercapacitive performance." *ACS Nano*, **12**, 1262 (2018).
53. K. Persson, Y. Hinuma, Y. S. Meng, A. Van der Ven, and G. Ceder, "Thermodynamic and kinetic properties of the Li-graphite system from first-principles calculations." *Phys. Rev. B*, **82**, 1254161 (2010).
54. D. A. Stevens and J. R. Dahn, "The mechanisms of lithium and sodium insertion in carbon materials." *J. Electrochem. Soc.*, **148**, A803 (2001).
55. J. P. Perdew and W. Yue, "Accurate and simple density functional for the electronic exchange energy: generalized gradient approximation." *Phys. Rev. B: Condens. Matter*, **33**, 8800 (1986).
56. J. P. Perdew, J. A. Chevary, S. H. Vosko, K. A. Jackson, M. R. Pederson, D. J. Singh, and C. Fiolhais, "Atoms, molecules, solids, and surfaces: applications of the generalized gradient approximation for exchange and correlation." *Phys. Rev. B: Condens. Matter*, **46**, 6671 (1992).
57. J. P. Perdew, K. Burke, and M. Ernzerhof, "Generalized gradient approximation made simple." *Phys. Rev. Lett.*, **77**, 3865 (1996).
58. M. Ernzerhof and G. E. Scuseria, "Assessment of the Perdew–Burke–Ernzerhof exchange-correlation functional." *J. Chem. Phys.*, **110**, 5029 (1999).
59. G. Kresse and J. Furthmiiller, "Efficiency of ab-initio total energy calculations for metals and semiconductors using a plane-wave basis set." *Comput. Mater. Sci.*, **6**, 15 (1996).
60. G. Kresse and J. Furthmuller, "Efficient iterative schemes for ab initio total-energy calculations using a plane-wave basis set." *Phys. Rev. B*, **54**, 11169 (1996).
61. G. Kresse and D. Joubert, "From ultrasoft pseudopotentials to the projector augmented-wave method." *Phys. Rev. B*, **59**, 1758 (1999).
62. G. Makov and M. C. Payne, "Periodic boundary conditions in ab initio calculations." *Phys. Rev. B: Condens. Matter*, **51**, 4014 (1995).
63. P. E. Blochl, "Projector augmented-wave method." *Phys. Rev. B: Condens. Matter*, **50**, 17953 (1994).
64. S. Ehrlich, J. Moellmann, W. Reckien, T. Bredow, and S. Grimme, "System-dependent dispersion coefficients for the DFT-D3 treatment of adsorption processes on ionic surfaces." *ChemPhysChem*, **12**, 3414 (2011).
65. H. J. Monkhorst and J. D. Pack, "Special points for Brillouin-zone integrations." *Phys. Rev. B*, **13**, 5188 (1976).
66. G. Henkelman, B. P. Uberuaga, and H. Jonsson, "A climbing image nudged elastic band method for finding saddle points and minimum energy paths." *J. Chem. Phys.*, **113**, 9901 (2000).
67. S. NosÉ, "A molecular dynamics method for simulations in the canonical ensemble." *Mol. Phys.*, **100**, 191 (2002).
68. W. G. Hoover, "Canonical dynamics: equilibrium phase-space distributions." *Phys. Rev. A Gen. Phys.*, **31**, 1695 (1985).
69. K. T. Chan, J. B. Neaton, and M. L. Cohen, "First-principles study of metal adatom adsorption on graphene." *Phys. Rev. B*, **77**, 2354301 (2008).
70. P. Wang, S. M. Zakeeruddin, J. E. Moser, M. K. Nazeeruddin, T. Sekiguchi, and M. Gratzel, "A stable quasi-solid-state dye-sensitized solar cell with an amphiphilic ruthenium sensitizer and polymer gel electrolyte." *Nat. Mater.*, **2**, 402 (2003).
71. M. Wagemaker, R. van de Krol, A. P. M. Kentgens, A. A. van Well, and F. M. Mulder, "Two phase morphology limits lithium diffusion in TiO_2 (Anatase): a ^{7}Li MAS NMR study." *J. Am. Chem. Soc.*, **123**, 11454 (2001).
72. V. V. Kulish, O. I. Malyi, M.-F. Ng, P. Wu, and Z. Chen, "Enhanced Li adsorption and diffusion in silicon nanosheets based on first principles calculations." *RSC Adv.*, **3**, 4231 (2013).
73. T. Yu, Z. Zhao, L. Liu, S. Zhang, H. Xu, and G. Yang, "TiC_3 monolayer with high specific capacity for sodium-ion batteries." *J. Am. Chem. Soc.*, **140**, 5962 (2018).
74. G. A. Tritsaris, K. Zhao, O. U. Okeke, and E. Kaxiras, "Diffusion of lithium in bulk amorphous silicon: a theoretical study." *J. Phys. Chem. C*, **116**, 22212 (2012).
75. J. Zhou, J. Lian, L. Hou, J. Zhang, H. Gou, M. Xia, Y. Zhao, T. A. Strobel, L. Tao, and F. Gao, "Ultrahigh volumetric capacitance and cyclic stability of fluorine and nitrogen co-doped carbon microspheres." *Nat. Commun.*, **6**, 8503 (2015).
76. C. Eames and M. S. Islam, "Ion intercalation into two-dimensional transition-metal carbides: global screening for new high-capacity battery materials." *J. Am. Chem. Soc.*, **136**, 16270 (2014).
77. T. Huang, B. Tian, J. Guo, H. Shu, Y. Wang, and J. Dai, "Semiconducting borophene as a promising anode material for Li-ion and Na-ion batteries." *Mater. Sci. Semicon. Proc.*, **89**, 250 (2019).
78. S. Zhao, W. Kang, and J. Xue, "The potential application of phosphorene as an anode material in Li-ion batteries." *J. Mater. Chem. A*, **2**, 19046 (2014).
79. D. Wang, Y. Gao, Y. Liu, D. Jin, Y. Gogotsi, X. Meng, F. Du, G. Chen, and Y. Wei, "First-principles calculations of Ti2N and Ti_2NT_2 (T=O, F, OH) monolayers as

potential anode materials for lithium-ion batteries and beyond." *J. Phys. Chem. C*, **121**, 13025 (2017).
80. H. Lin, D.-D. Yang, N. Lou, S.-G. Zhu, and H.-Z. Li, "Functionalized titanium nitride-based MXenes as promising host materials for lithium-sulfur batteries: a first principles study." *Ceram. Int.*, **45**, 1588 (2019).
81. N. K. Jena, R. B. Araujo, V. Shukla, and R. Ahuja, "Borophane as a benchmate of graphene: a potential 2D material for anode of Li and Na-ion batteries." *ACS Appl. Mater. Interfaces*, **9**, 16148 (2017).
82. Y. Liu, V. I. Artyukhov, M. Liu, A. R. Harutyunyan, and B. I. Yakobson, "Feasibility of lithium storage on graphene and its derivatives." *J. Phys. Chem. Lett.*, **4**, 1737 (2013).
83. J. Hu, B. Xu, C. Ouyang, S. A. Yang, and Y. Yao, "Investigations on V_2C and V_2CX_2 (X=F, OH) monolayer as a promising anode material for Li ion batteries from first-principles calculations." *J. Phys. Chem. C*, **118**, 24274 (2014).
84. B. Mortazavi, M. Shahrokhi, M. E. Madjet, M. Makaremi, S. Ahzi, and T. Rabczuk, "N-, P-, As-triphenylene-graphdiyne: strong and stable 2D semiconductors with outstanding capacities as anodes for Li-ion batteries." *Carbon*, **141**, 291 (2019).
85. T. Zhang, Y. Ma, B. Huang, and Y. Dai, "Two-dimensional penta-BN_2 with high specific capacity for Li-ion batteries." *ACS Appl. Mater. Interfaces*, **11**, 6104 (2019).
86. D. Wu, B. Yang, H. Chen, and E. Ruckenstein, "Nitrogenated holey graphene C_2N monolayer anodes for lithium- and sodium-ion batteries with high performance." *Energy Storage Mater.*, **16**, 574 (2019).
87. H. Lin, R. Jin, A. Wang, S. Zhu, and H. Li, "Transition metal embedded C_2N with efficient polysulfide immobilization and catalytic oxidation for advanced lithium-sulfur batteries: a first principles study." *Ceram. Int.*, **45**, 17996 (2019).
88. R. Bhuvaneswari, V. Nagarajan, and R. Chandiramouli, "Germanene nanosheets as a novel anode material for sodium-ion batteries—a first-principles investigation." *Mater. Res. Express*, **6**, 0355041 (2018).
89. A. Sengupta and T. Frauenheim, "Lithium and sodium adsorption properties of monolayer antimonene." *Mater. Today Energy*, **5**, 347 (2017).
90. D. Er, J. Li, M. Naguib, Y. Gogotsi, and V. B. Shenoy, "Ti_3C_2 MXene as a high capacity electrode material for metal (Li, Na, K, Ca) ion batteries." *ACS Appl. Mater. Interfaces*, **6**, 11173 (2014).
91. F. Li, Y. Qu, and M. Zhao, "Germanium sulfide nanosheet: a universal anode material for alkali metal ion batteries." *J. Mater. Chem. A*, **4**, 8905 (2016).
92. Q. Tang, Z. Zhou, and P. Shen, "Are MXenes promising anode materials for Li ion batteries? Computational studies on electronic properties and Li storage capability of Ti_3C_2 and $Ti_3C_2X_2$ (X=F, OH) monolayer." *J. Am. Chem. Soc.*, **134**, 16909 (2012).
93. X. Zhang et al., "Absorption and diffusion of lithium on layered InSe." *Comput. Condens. Matter*, **21**, e004041 (2019).
94. T. Bo, P. F. Liu, J. Zhang, F. Wang, and B. T. Wang, "Tetragonal and trigonal Mo_2B_2 monolayers: two new low-dimensional materials for Li-ion and Na-ion batteries." *Phys. Chem. Chem. Phys.*, **21**, 5178 (2019).
95. E. Yang, H. Ji, and Y. Jung, "Two-dimensional transition metal dichalcogenide monolayers as promising sodium ion battery anodes." *J. Phys. Chem. C*, **119**, 26374 (2015).